Figure S1 Variations in clear-sky shortwave aerosol radiative effects based on different amplitudes of total AOD (100% - 1000%) at 22.5°N – 25°N, 87.5°E – 90°E for (a) TOA flux, (b) surface flux, and (c) heating rate at the tropopause (100 hPa) at 0:00, 3:00, 6:00, 9:00, 12:00, 15:00, 18:00, 21:00 separately . Dotted lines show linear trends extrapolated from the 10% change between 100% and 110% of total AOD. Perturbations to AOD are uniform within the column.
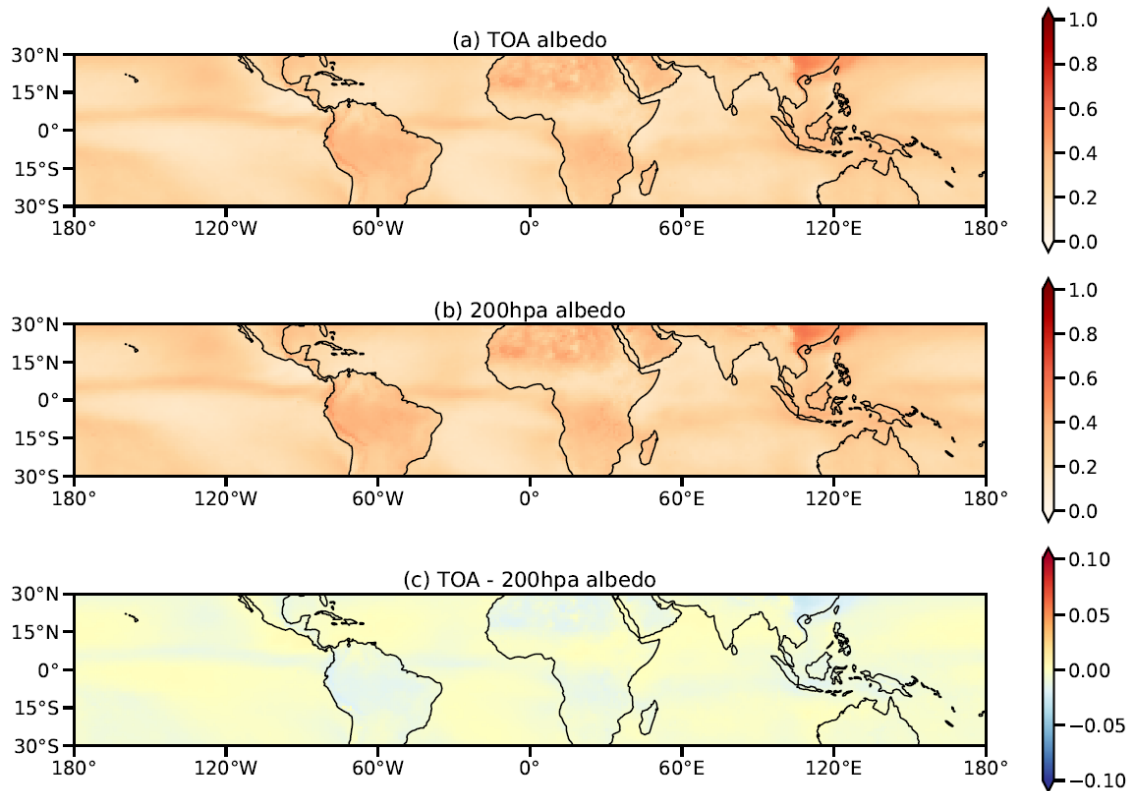
Figure S2 Distributions of (a) planetary albedo at TOA, (b) albedo at 200 hPa, and (c) the difference of (a) and (b). Data are averaged over 2011 – 2020 from CERES SYN1Deg.
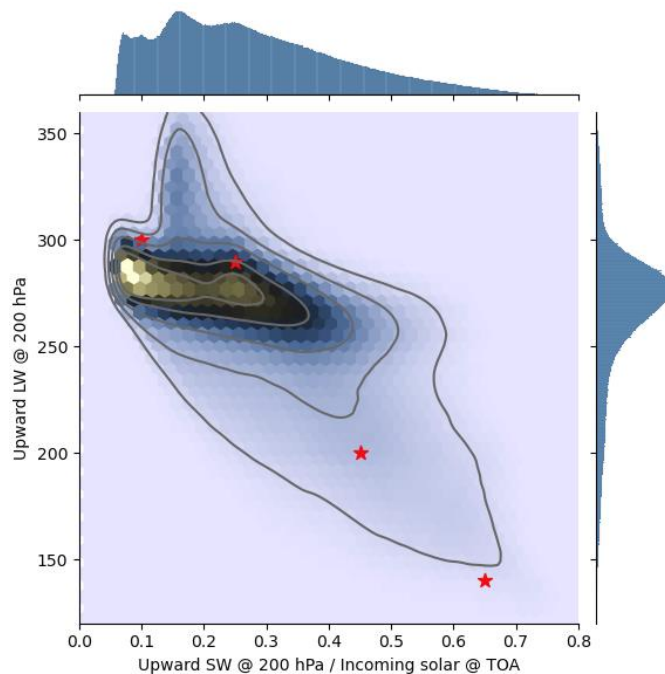
Figure S3 Joint plots of hourly albedo (*x*-axis) and longwave upward flux (*y*-axis) for 1° grid cells around 30°S in May during 2011 – 2020. Red stars indicate points chosen as representative reference state boundary conditions for the aerosol kernels.
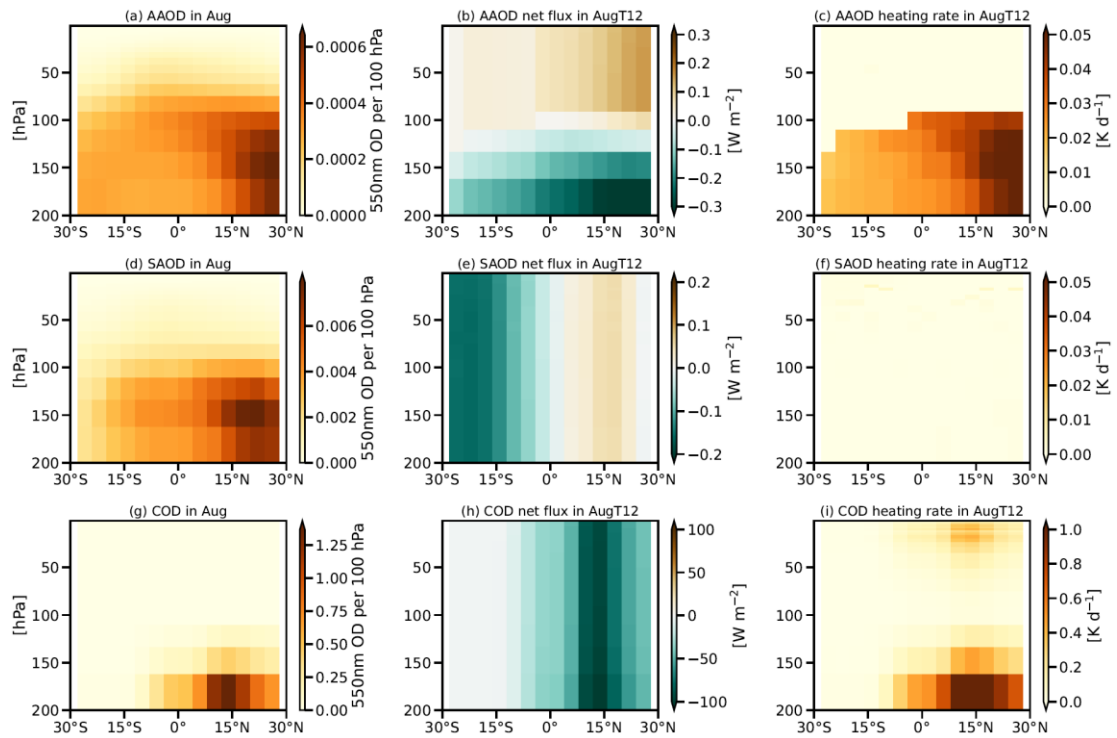
Figure S4 (a, d, g) optical depth, (b, e, h) radiative effect on shortwave net flux, and (c, f, i) radiative effect on shortwave heating by (a-c) absorbing aerosol, (d-f) scattering aerosol, and (g-i) cloud ice at 12:00 local solar time in August.
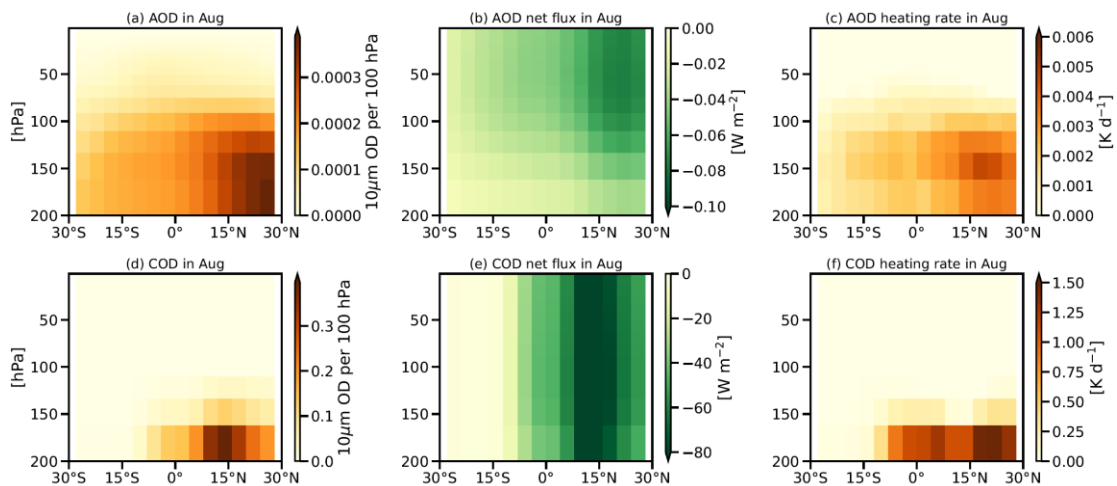
Figure S5 (a, d) optical depth at 10 μm, (b, e) radiative effect on longwave net upward flux, and (c, f) radiative effect on longwave heating by (a-c) absorbing aerosol and (d-f) cloud ice in August based on data from 2011 – 2020.
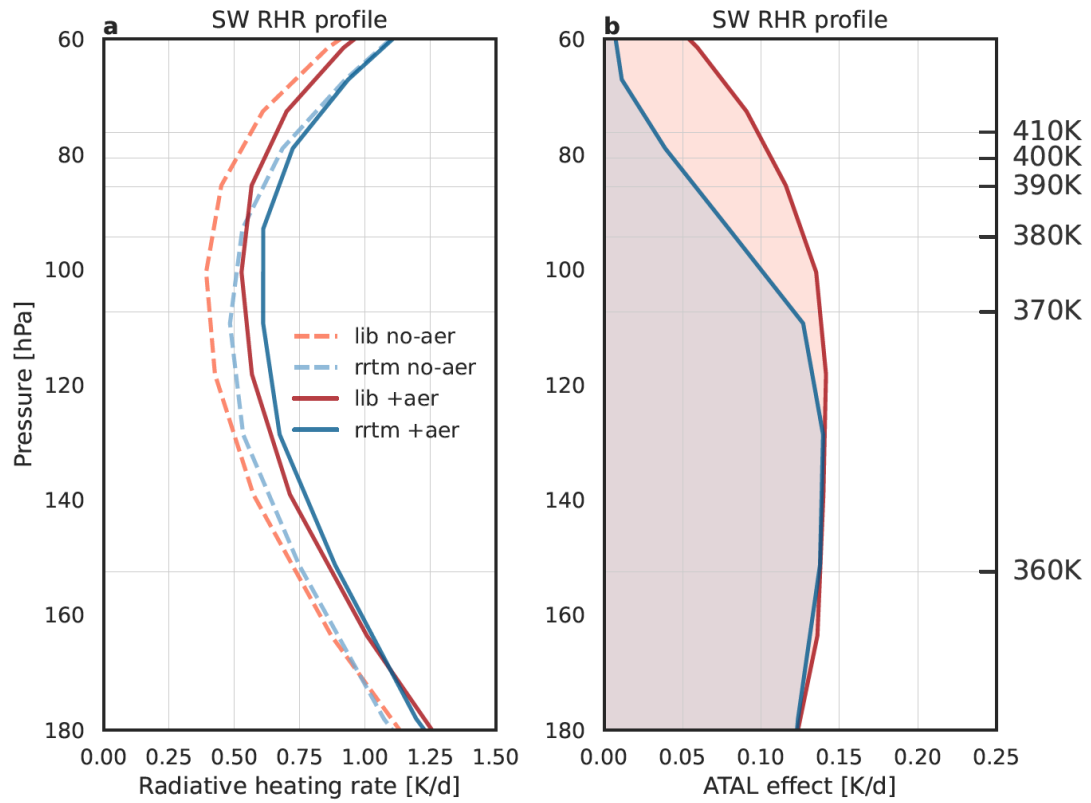
Figure S6 Vertical profiles of (a) clear-sky shortwave radiative heating within the UTLS calculated by libRadtran (red lines) and RRTMG_SW (blue lines) under pristine conditions (dashed lines) and with ATAL base profiles included (solid lines) above the ASM core region. (b) ATAL effects calculated by libRadtran (red) and RRTMG_SW (blue).